Electronic Supplementary Material (ESI) for Journal of Materials Chemistry A.


Supplementary Information

# Fabrication of Dianthracene-based Hyper-cross-linked Polymers for Selective Photocatalytic Oxidation of Organic Sulfides

*Ze-Jiu Diao, Guan-Zhou Wu, Tian-Jing Zhang, Hang-Ou Qi, Jing-Jing Li, Ming Lu, Guoliang Liu,* Xiao-Qin Liu, and Lin-Bing Sun**

State Key Laboratory of Materials-Oriented Chemical Engineering, Jiangsu National Synergetic Innovation Center for Advanced Materials (SICAM), College of Chemical Engineering, Nanjing Tech University, Nanjing 211816, China

* Corresponding authors. E-mail: glliu@njtech.edu.cn; lbsun@njtech.edu.cn

## 1. Chemicals and reagents

Anthracene (99%, Acros), 9-bromoanthracene (96%, Macklin), anhydrous aluminum trichloride (≥99.0%, Greagent), 1,4-diazabicyclo[2.2.2]octane (98%, Adamas), p-benzoquinone (99%, Acros), 5,5-dimethyl-1-pyrroline N-oxide (TCI, 97% GC&T), 2,2,6,6-tetramethyl-1-piperidinyloxy (Accela, 97% GC&T), thioanisole and its derivatives (Adamas, 99%), deuterated chloroform (Adamas, 99.8%D+0.03%TMS), deuterated dimethyl sulfoxide (Adamas, 99.9%D+0.03%TMS) were purchased from corresponding suppliers. Tetrahydrofuran (THF), methanol (MeOH), acetone, dichloromethane (DCM), N, N-Dimethylformamide (DMF), deionized water and 37% concentrated hydrochloric acid (HCl) were purchased as the reagent grade from Sinopharm Chemical Reagent Shanghai Co., Ltd. and used as received unless otherwise noted. 365 nm UV light (10 W, from Zigu Lighting Electrical Factory) and 420 nm LED (20 W, from Xuzhou Aijia Electrical Technology) were used for irradiation.

## 2. Experimental Methods

### 2.1 Synthesis of DiAn

The synthesis procedure of 5,6,11,12-tetrahydro-5,12:6,11-bis([1,2]benzeno)dibenzo[a,e][8] annulene (DiAn) was modified on the basis of previous literature (Scheme S1). Anthracene (2 g, 11.2 mmol) was dissolved in 50 mL degassed tetrahydrofuran, and then the pale yellow solution was transferred into a degassed quartz tube. After that, 365 nm UV light was used to irradiate the solution for 8 h at room temperature, and the solution slowly turned to turbid in this process. The product was obtained by filtration when the suspended solid stopped occurring. Deionized water and methanol were used to wash the crude product successively before the white powder was dried at 60 $^{o}$C in a vacuum oven. Finally, 1.13 g white product was obtained, with a yield of 56%. $^{1}$H NMR (400 MHz, deuterated dimethyl sulfoxide, 298 K) δ 6.94 (dd, J = 5.5, 3.3 Hz, 2H), 6.77 (dd, J = 5.4, 3.2 Hz, 2H), 4.62 (s, 1H). (Fig. S3)

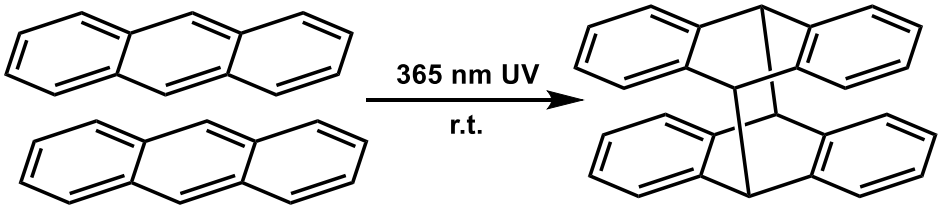


**Scheme S1.** The synthesis route for DiAn.

## 2.2 Synthesis of DiBrAn

The synthesis procedure of 5,11-dibromo-5,6,11,12-tetrahydro-5,12:6,11-bis([1,2]benzeno) dibenzo[a,e][8]annulene (DiBrAn) was carried out as follows. 9-Bromoanthracene (2 g, 7.7 mmol) was dissolved in 15 mL degassed tetrahydrofuran, and then the yellow solution was transferred into a degassed quartz tube. After that, 365 nm UV light was used to irradiate the solution for 6 hours at room temperature, and the solution slowly turned turbid in this process. The product was obtained by filtration when the suspended solid stopped occurring. Deionized water and methanol were used to wash the crude product successively before the white powder was dried at 60 ºC in a vacuum oven. Finally, 1.45 g white product was obtained, with a yield of 72%. $^{1}$H NMR (400 MHz, deuterated chloroform, 298 K) δ 7.77 (dd, J = 7.6, 1.3 Hz, 2H), 7.06-6.82 (m, 6H), 5.33 (s, 1H). (Fig. S4) $^{13}$C NMR (101 MHz, deuterated chloroform, 298 K) δ 142.54, 138.55, 128.19, 127.48, 127.12, 126.72, 76.09, 68.89. (Fig. S5)

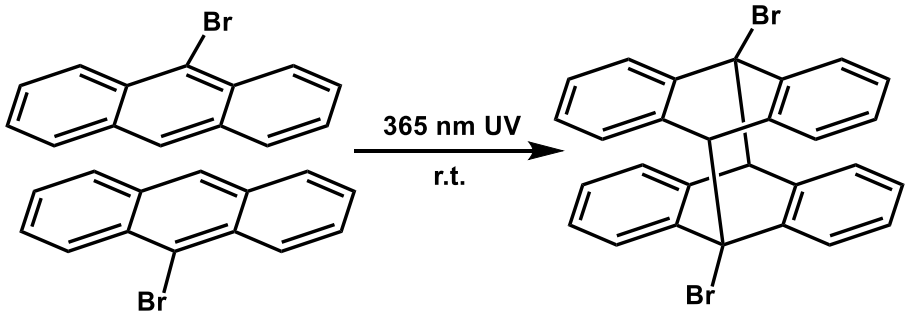


**Scheme S2.** The synthesis route for DiBrAn.

## 2.3 Recrystallization experiment for DiBrAn

10 mg DiBrAn was dispersed in 8 mL DMF and heated at 80 ºC until the solution became clear. The vial equipped with solution stood at room temperature for 24 h and then block crystals of size larger than 100 μm would be obtained.

## 2.4 HCP-DiAn synthesis

DiAn (356 mg, 1 mmol) was placed in a 50 mL ball mill pot, and then 1,3,5-tris(bromomethyl)benzene (500 mg, 1.4 mmol) and anhydrous $AlCl_3$ (500 mg, 3.75 mmol) were mixed with DiAn. After that, 2~3 drops of DCM were instilled into the ball mill pot and the pot was sealed immediately. When balancing was completed, the ball mill pot was transferred into the

machine and rotated at 500 rpm for 30 min. Once the reaction finished, the black crude product was fully washed by hydrochloric acid, MeOH, acetone, and DCM respectively. The product was purified through a Soxhlet extractor in methanol for 24 h in order to remove the residual catalyst and monomer. Finally, the product was obtained as a brownish powder after drying under reduced pressure at 80 °C for 24 h, with a yield of 62.5 %. Elemental combustion analysis (%) Calcd for $(C_{126}H_{108})n$: C 93.29%; H 6.71%; Found: C 88.10%; H 5.38%.

### 2.5 HCP-DiBrAn synthesis

DiBrAn (514 mg, 1 mmol) and 1,3,5-tris(bromomethyl)benzene (500 mg, 1.4 mmol) were dissolved in 50 mL DCM and poured into a 250 mL three-necked flask. The flask was bubbled for 30 min by nitrogen to exclude oxygen, and then anhydrous $AlCl_3$ (500 mg, 3.75 mmol) was added to the solution. The reaction was carried out at 40 ºC for 24 h and in this process, the color of the solution slowly deepened. Once the reaction finished, the black crude product was fully washed by hydrochloric acid, MeOH, acetone, and DCM respectively. The product was purified through a Soxhlet extractor in MeOH for 24 h in order to remove all the residual catalyst and monomer. Finally, the product was obtained as a dark brownish powder after drying under reduced pressure at 80 °C for 24 h, with a yield of 87.5 %. Elemental combustion analysis (%) Calcd for $(C_{126}H_{102}Br_6)n$: C 72.22%; H 4.91%; Found: C 70.80%; H 5.31%.

### 2.6 Characterization

$^1H$ NMR spectra were recorded at room temperature on a Bruker Avance 400 MHz spectrometer. Chemical shifts are given in ppm with respect to TMS. Solid-state $^{13}C$ cross-polarization magic-angle spinning (CP/MAS) NMR spectra of the sample were conducted at 14.01 T using a JNM-ECZ600R spectrometer (JEOL RESONANCE Inc., Japan) operating at a $^1H$ resonance frequency of 599.7 MHz. The rotational speed was set as 12kHz and the scanning time was 1 hour. Fourier transform infrared (FT-IR) spectra were recorded on KBr (1:30, w/w) pellets in the 4000-600 $cm^{-1}$ range using a Perkin-Elmer Spectrum One FT-IR spectrometer. Elemental analyses (C, H, and N) were performed on an Elementar Unicube elemental analyzer. UV-Visible diffuse reflectance spectra (UV-Vis DRS) were performed on Shimadzu UV-3600 PLUS and the test range is from 200 to 800 nm using $BaSO_4$ as a reference. $N_2$ adsorption-desorption isotherms were measured using BELSORP-MAX analyzer at 77 K. The samples were degassed at 80 ºC for 12 h prior to analysis. The Brunauer-Emmett-Teller (BET) surface area was calculated using adsorption data in a relative pressure ranging from 0.05 to 0.30.

The pore diameter was calculated from the adsorption branch by using the no-local density functional theory (NLDFT) method. Thermogravimetric analysis (TGA) curves were obtained by use of a thermobalance (STA-499C, NETZSCH). The sample was heated from room temperature to 800 °C with a heating rate of 5 °C $min^{-1}$ under a flow of $N_2$ (20 mL $min^{-1}$). Powder X-ray diffraction (PXRD) patterns were collected on a Bruker D8 Avance S5 diffractometer with Cu Kα radiation at 40 kV and 40 mA. Scanning Electron Microscopy (SEM) experiments were carried out on a Hitachi Regulus8100 at 3 kV equipped with an energy dispersive spectrometer (EDS, Oxford Instruments, 80 mm2 detector). Samples were treated via Pt sputtering before observation. The electron paramagnetic resonance (EPR) experiments were conducted on an electron paramagnetic resonance spectrometer (JEOL, JES-FA300). Single crystal X-ray diffraction analysis was collected on a Bruker APEX-II CCD diffractometer with graphite-monochromated Cu Kα radiation (λ=1.54178).

Photoelectrochemical measurements were performed on an electrochemical workstation (CHI 660E, CH Instruments Inc., Shanghai) in a standard three-electrode system. The photocatalyst-coated glassy carbon (Φ = 3 cm) was chosen as the working electrode, an Ag/AgCl electrode was applied as a reference electrode, and Pt wire was used as the counter electrode. The electrolyte is a 0.1 M $Na_2SO_4$ aqueous solution. The samples (10 mg) were dispersed into 1 mL ethanol with 50 μL Nafion mixed solution, and the working electrode was prepared by dropping the suspension onto the surface of the glassy carbon electrode and drying repeatedly (10 μL × 15). The photocurrents were recorded under the 420 nm LED light switching every 20 seconds and 0.5 M $Na_2SO_4$ solution was chosen as a primer. Electrochemical impedance spectroscopy measurement was performed in the range of 0.1 Hz-100 KHz without light irradiation and the electrolyte was 2.5 mM potassium solution. Mott-Schottky analysis was executed at the frequency of 1000 Hz and the potential range was set between -1 and 1 V on the basis of 0.5 M $Na_2SO_4$ solution. Hall measurement was conducted by Ecopia HMS-7000 and the magnetic field strength is set to 0.5 T. The transient surface photovoltage (TSPV) spectrometer was carried out on a homemade instrument using a nanosecond laser (YAG: Q-smart 450, 120 J, 355 nm) as an excitation resource and an oscilloscope (TDS Tektronix 5054, 500 MHz) as a signal collector.

### 2.6 The typical procedure for the photocatalytic oxidation of sulfides

At the start, add 0.5 mmol of sulfide and 5 mg of **HCP-DiAn** and **HCP-DiBrAn** into a 10 mL Pyrex reactor containing 1 mL of MeOH as the solvent. The mixture was stirred for half an hour to achieve adsorption-desorption equilibrium under the dark condition. Next, the Pyrex reactor was sealed and filled with air to 0.1 MPa. Afterward, the Pyrex reactor was magnetically stirred at a speed

of 1500 rpm for 3h. In the end, the photocatalyst was separated from the reaction mixture by centrifugation and the product was left in the solvent MeOH.

The product phenyl methyl sulfoxide and its derivatives were characterized quantitatively and qualitatively by $^1$H NMR. The detailed process is described as follows. The solvent was evaporated at room temperature and the product with high boiling point (usually higher than 120 $^o$C) remained. Subsequently, the product was dissolved in deuterated chloroform for $^1$H NMR analysis. $^1$H NMR result reveals that the products have different characteristic peaks, which can be identified according to previously reported literature[1]. The integral values of each characteristic peak were calculated. After that, the conversion and selectivity can also be obtained according to the ratio of the integral value of characteristic peaks.

### 2.7 Recycle experiments for the photocatalytic oxidation of sulfides

After the first run reaction was finished, the catalyst was recovered by centrifugation, and then washed thoroughly with MeOH to remove any residual products or unreacted substrates. The catalyst was dried under vacuum at 80 $^o$C for 2 h. The recovered catalyst was re-employed in the next cycle under identical conditions.

### 2.8 Calculation model of pore width distribution

Traditional calculation models of pore width distribution include Horvath-Kawazoe (HK), Saito-Foley (SF), Barret-Joyner-Halenda (BJH) and so on. These models mainly rely on experience and only suitable for one type of pore width. According to the $N_2$ adsorption-desorption isotherms of HCPs at 77 K, the uptake increase rapidly at low pressure and unclosed hysteresis loop exists at middle pressure, implying that HCPs possess more than one pore width types. In this case, non-local density functional theory (NLDFT) model is chosen to calculated pore width distribution due to its universality. We use the software of BELMaster (Version 7.0.18.8) that comes with BELSORP-MAX analyzer to conduct the calculation and the parameters are set as follows.

| Interpolate curves | Kernel | Adsorptive/ Temp | Model | Adsorbent | Data select | Fitting method | Definition of pore width |
|---|---|---|---|---|---|---|---|
| 3 dimension spline | NLDFT | $N_2$/77K | Slit | Graphitic carbon | Ads. | Log-normal (5) | Solid definition |

## 2.9 DFT computational details

The theoretical calculations were performed via the Gaussian 16 suite of programs. The structures of the studied molecules were fully optimized at the B3LYP-D3BJ/def2-SVP level of theory. The vibrational frequencies of the optimized structures were carried out at the same level. The structures were characterized as a local energy minimum on the potential energy surface by verifying that all the vibrational frequencies were real. The molecular orbital levels of studied compounds were investigated via theoretical calculations, including the highest occupied molecular orbital (HOMO) and the lowest unoccupied molecular orbital (LUMO). The GaussView package was used to plot the color-filled iso-surface graphs to visualize the molecular orbitals.

## 3. Additional Figures

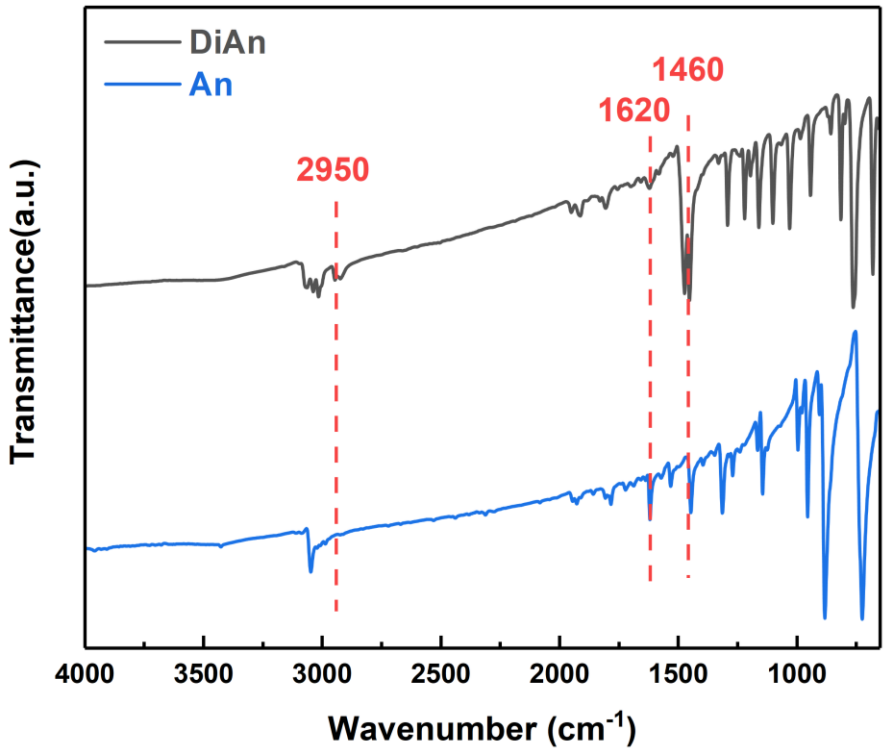


**Fig. S1** FT-IR spectra of An and DiAn.

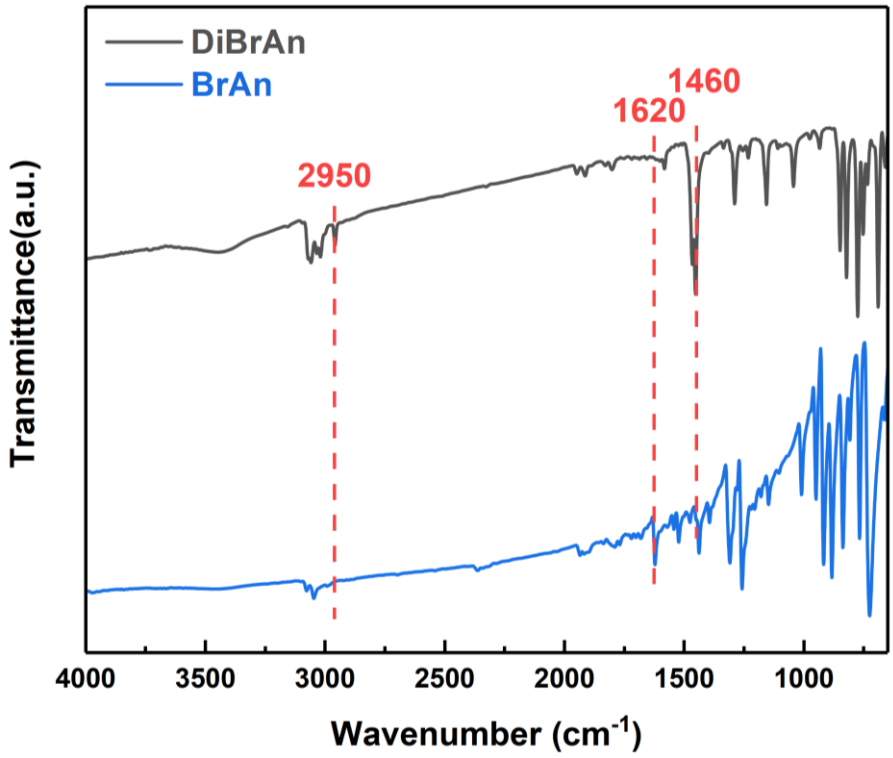


**Fig. S2** FT-IR spectra of BrAn and DiBrAn.

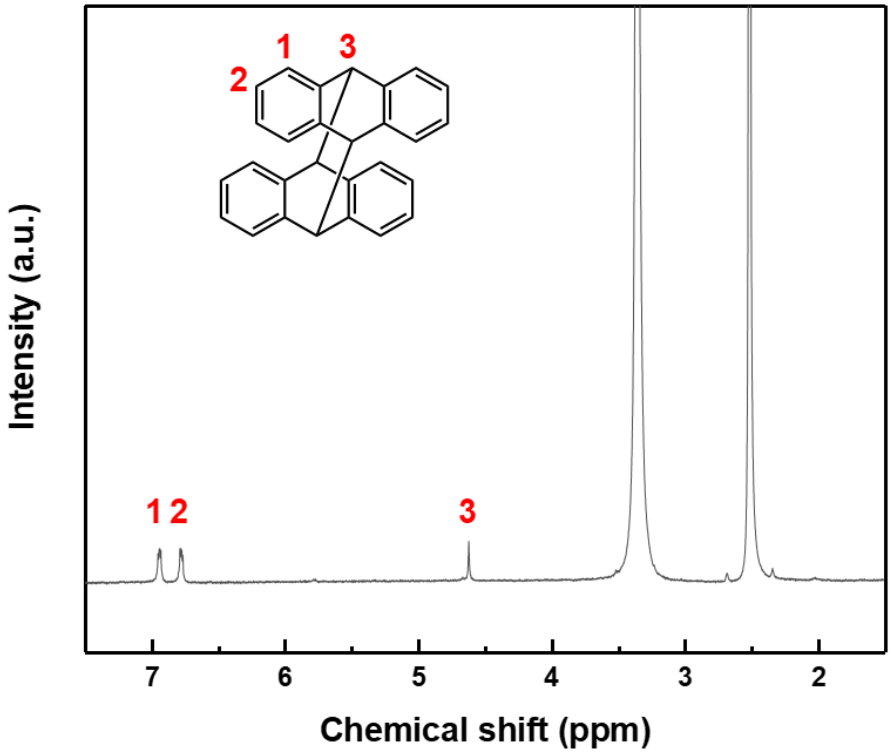


**Fig. S3** $^{1}$H NMR analysis of DiAn.

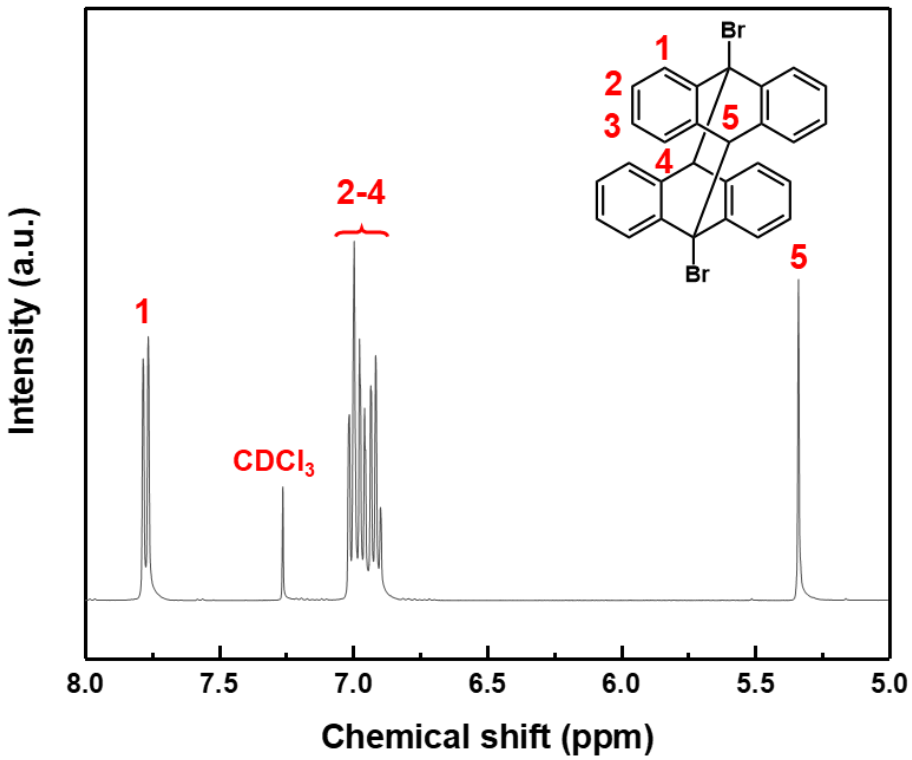


**Fig. S4** $^{1}$H NMR analysis of DiBrAn.

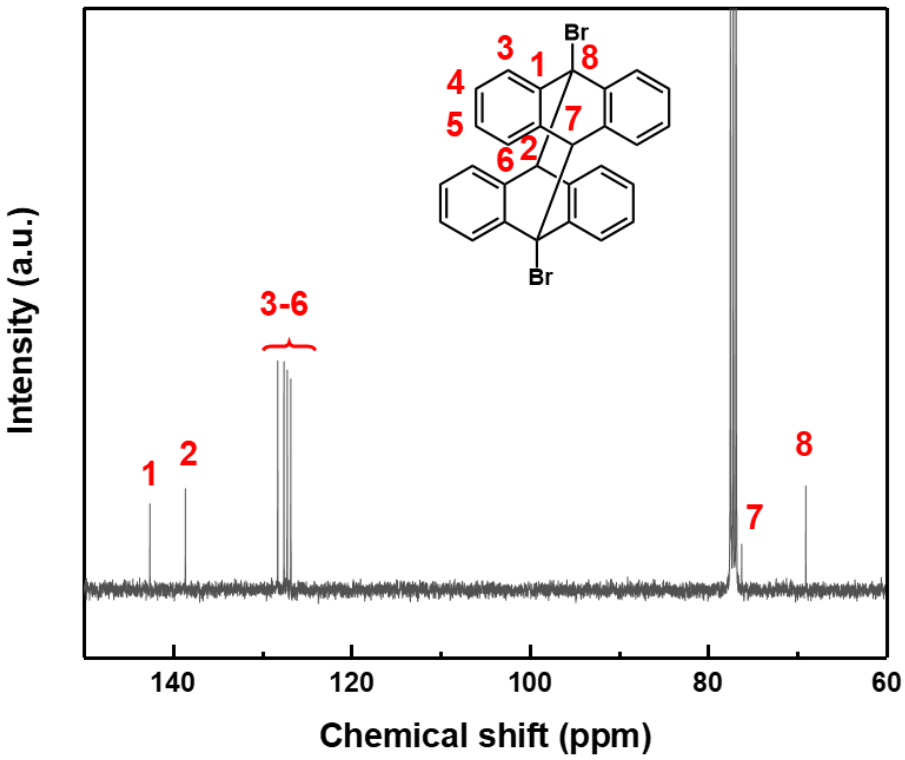


**Fig. S5** $^{13}$C NMR analysis of DiBrAn.

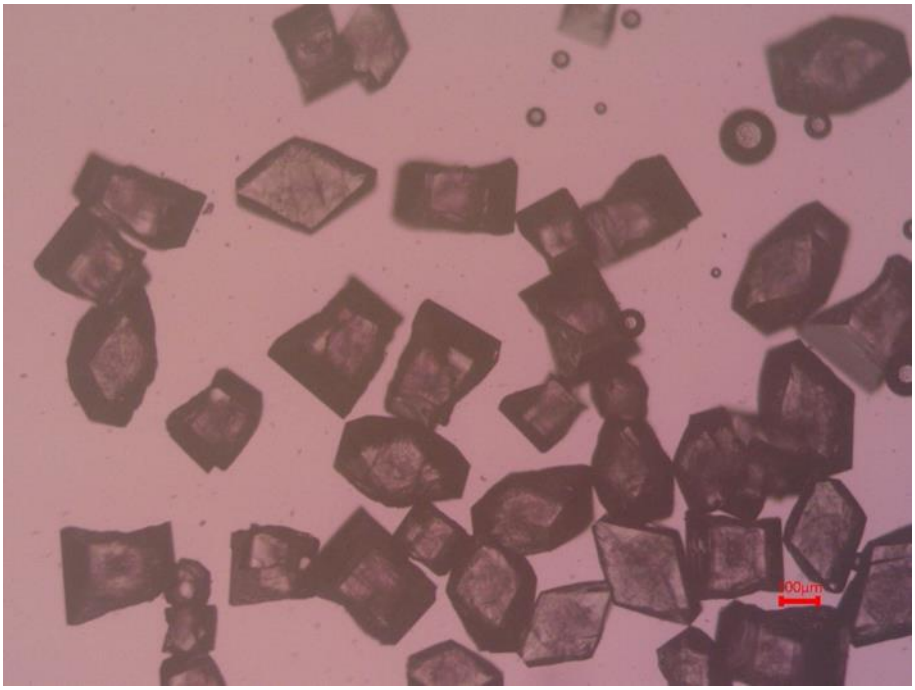


**Fig. S6** Opotical microscope image of DiBrAn crystals.

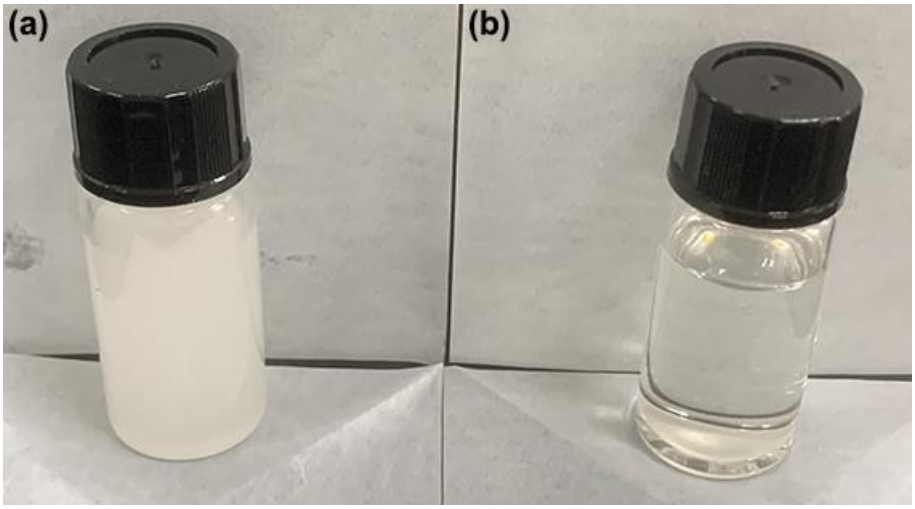


**Fig. S7** The solubility difference between (a) DiAn and (b) DiBrAn in DCM.

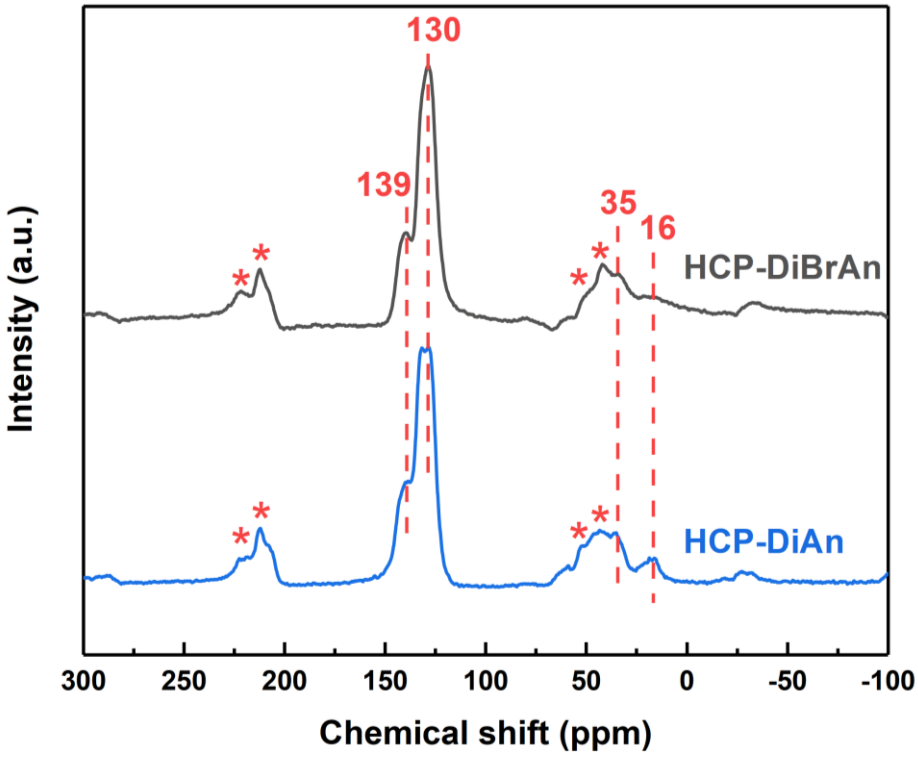


**Fig. S8** Experimental $^{13}C$ CP-MAS NMR spectra of HCP-DiAn and HCP-DiBrAn. Asterisks denote spinning sidebands.

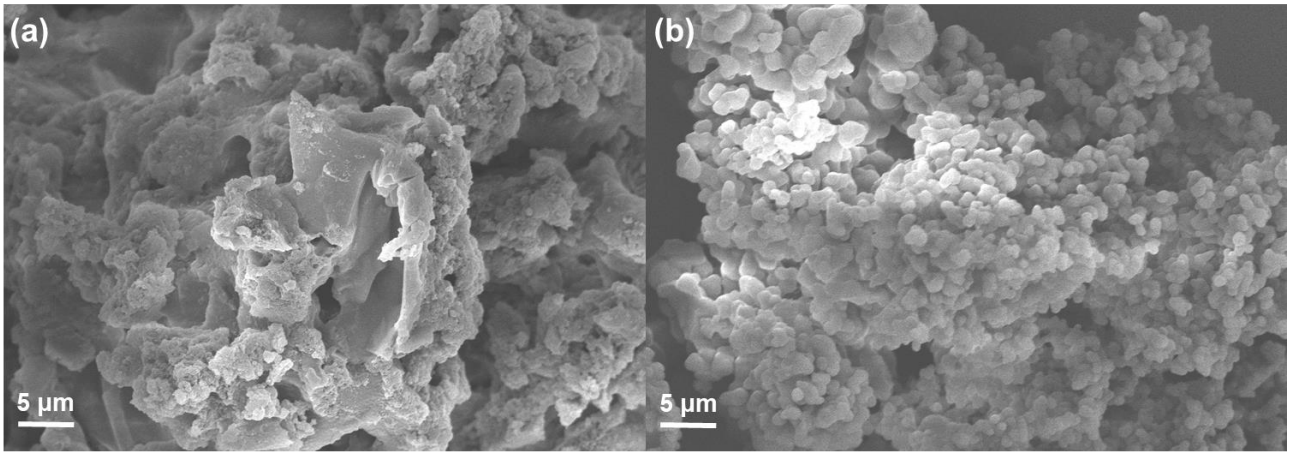


**Fig. S9** SEM images for (a) HCP-DiAn and (b) HCP-DiBrAn.

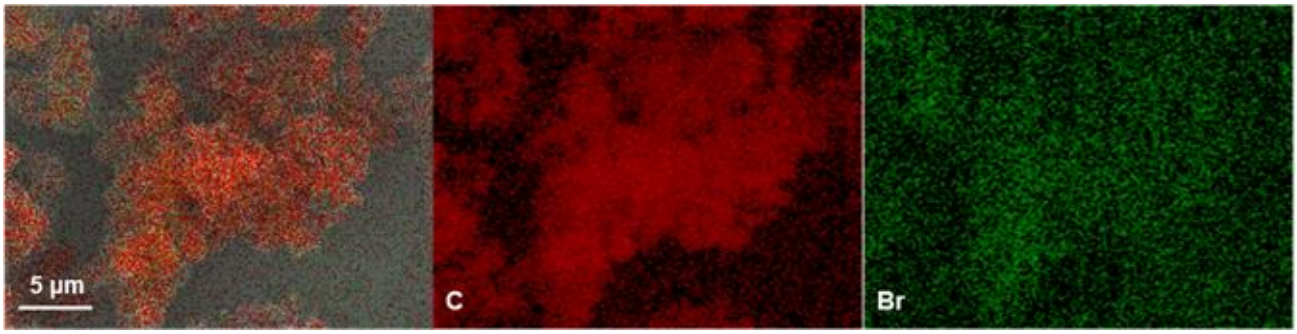


**Fig. S10** EDX mapping images of C and Br elements of HCP-DiBrAn.

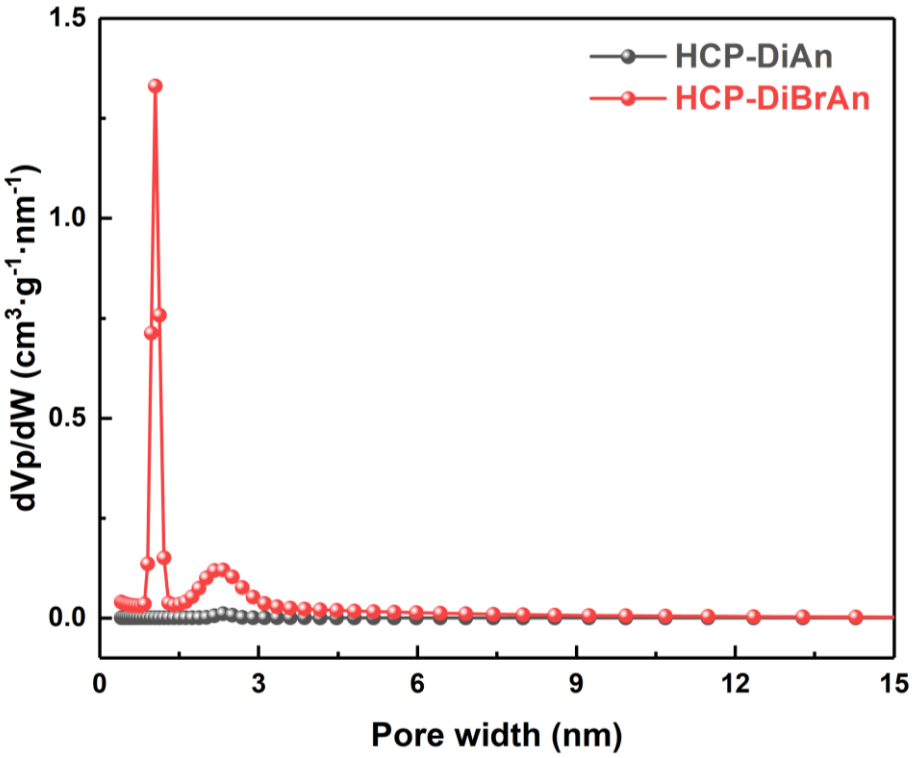


**Fig. S11** Pore size distributions of HCP-DiAn and HCP-DiBrAn.

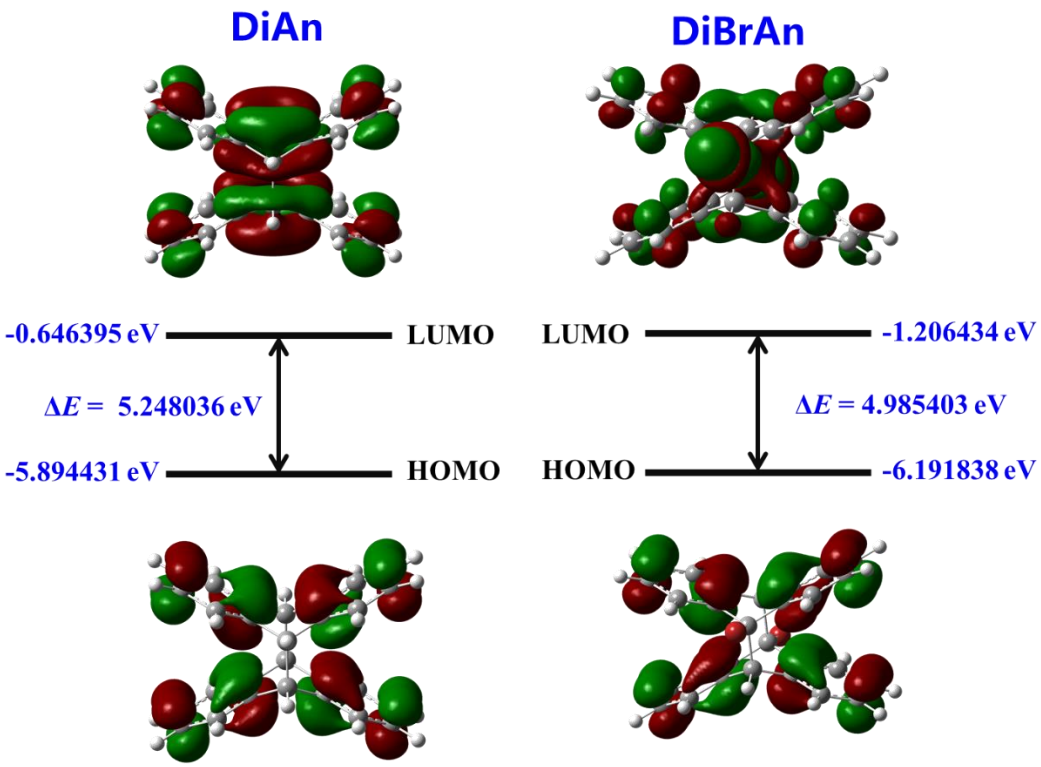


**Fig. S12** DFT calculation of molecular orbital levels of DiAn and DiBrAn.

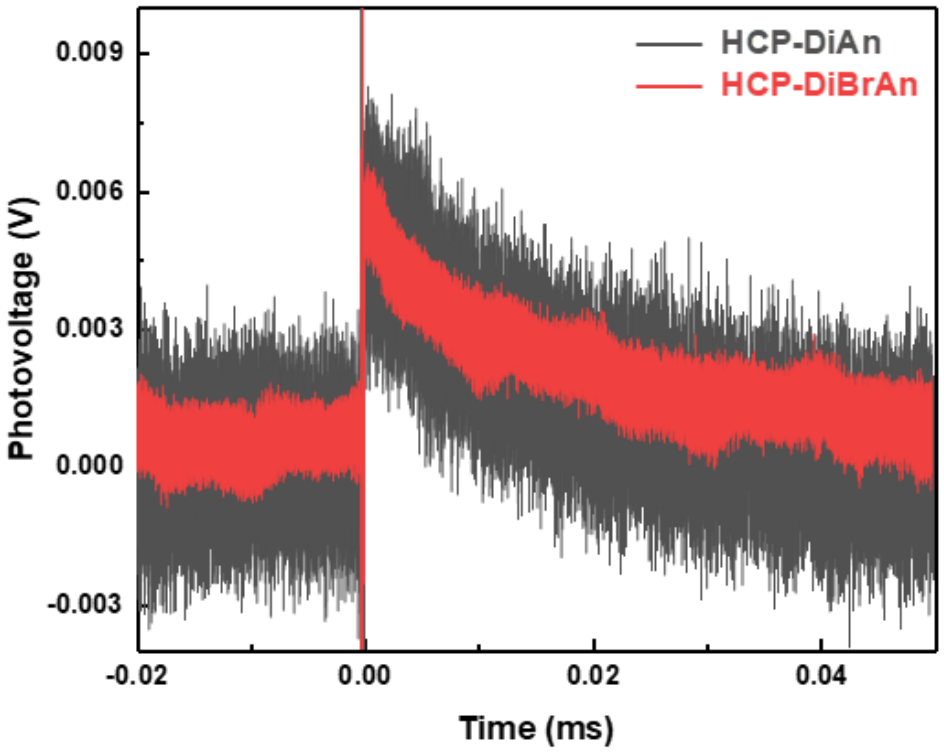


**Fig. S13** Transient surface photovoltage spectra of HCP-DiAn and HCP-DiBrAn.

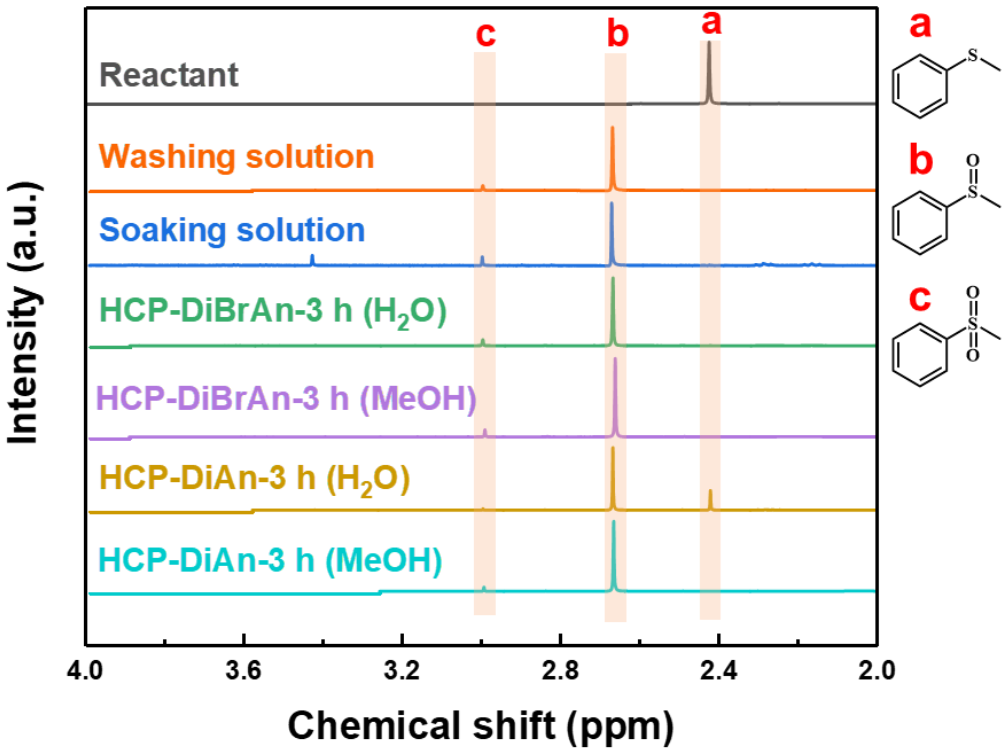


**Fig. S14** $^{1}$H NMR spectra of oxidative products under different conditions.

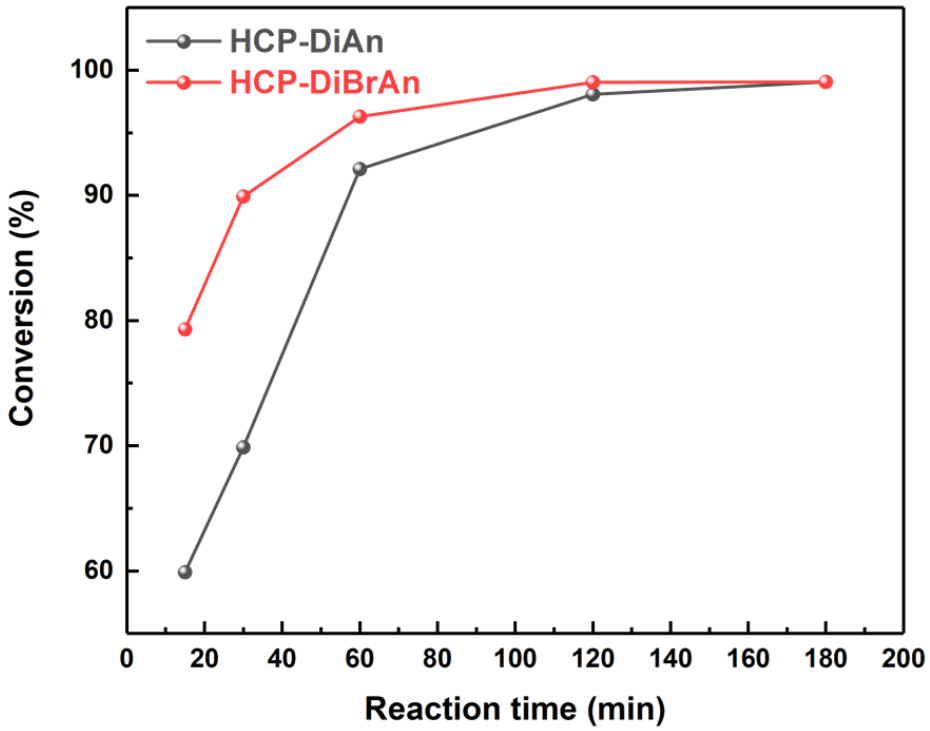


**Fig. S15** Conversion of methylphenyl sulfide in the presence of HCP-DiAn and HCP-DiBrAn.

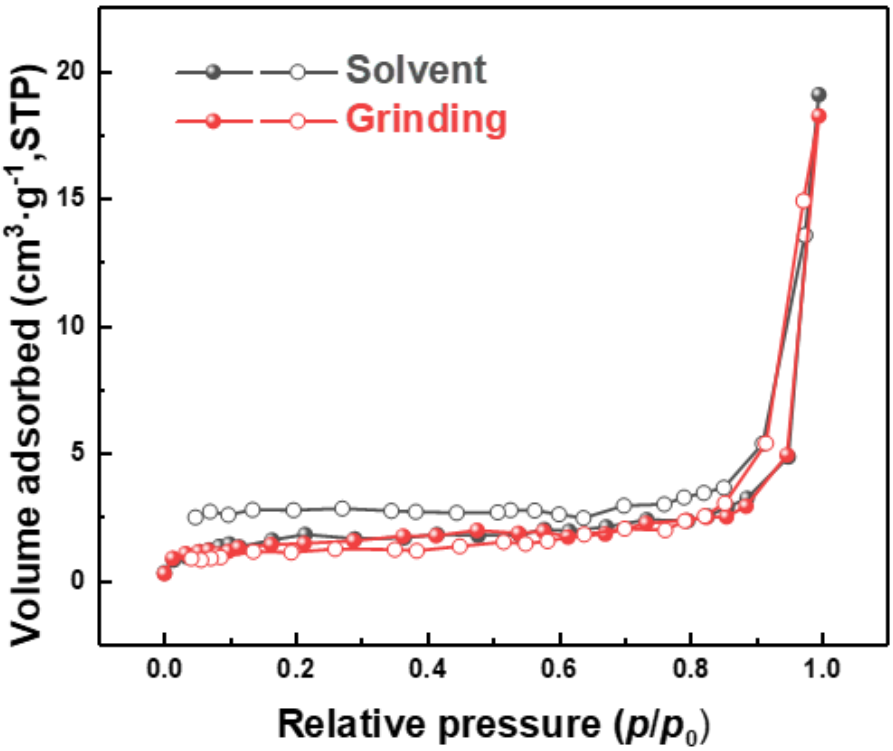


**Fig. S16** $N_2$ sorption isotherms at 77 K of HCP-DiAn synthesized by different methods.

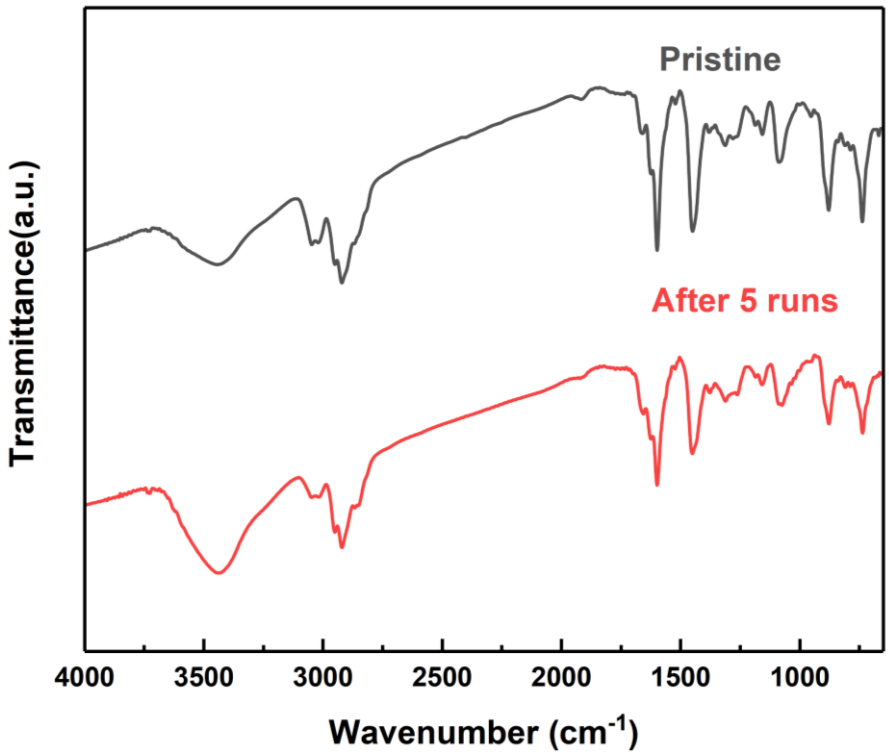


**Fig. S17** FT-IR analysis of HCP-DiBrAn after performance evaluation for 5 runs.

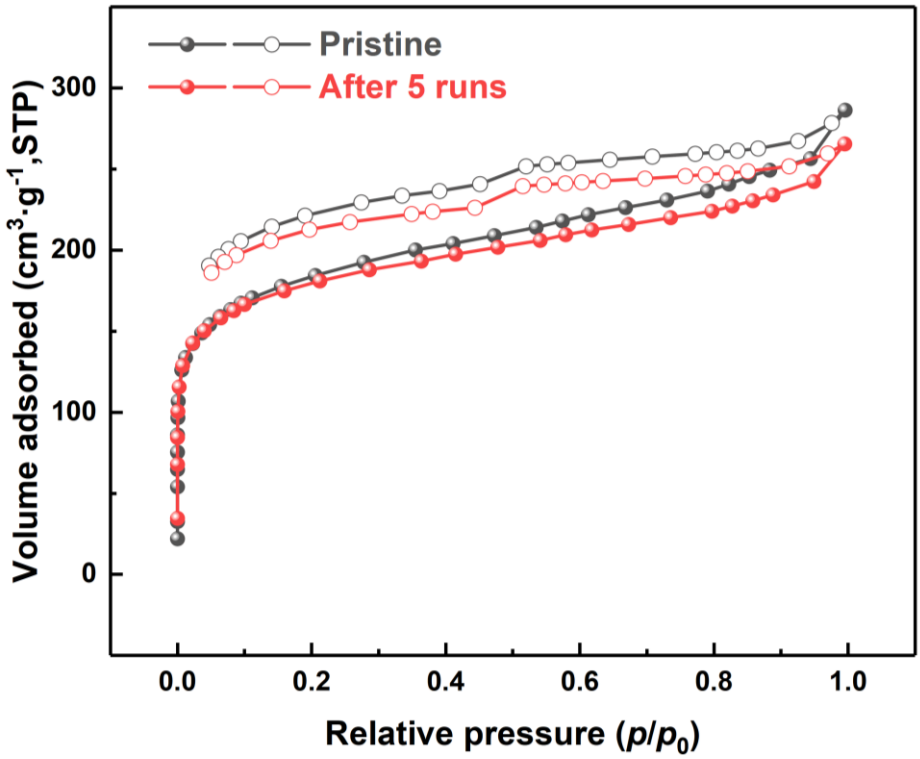


**Fig. S18** $N_2$ uptake analysis of HCP-DiBrAn after performance evaluation for 5 runs.

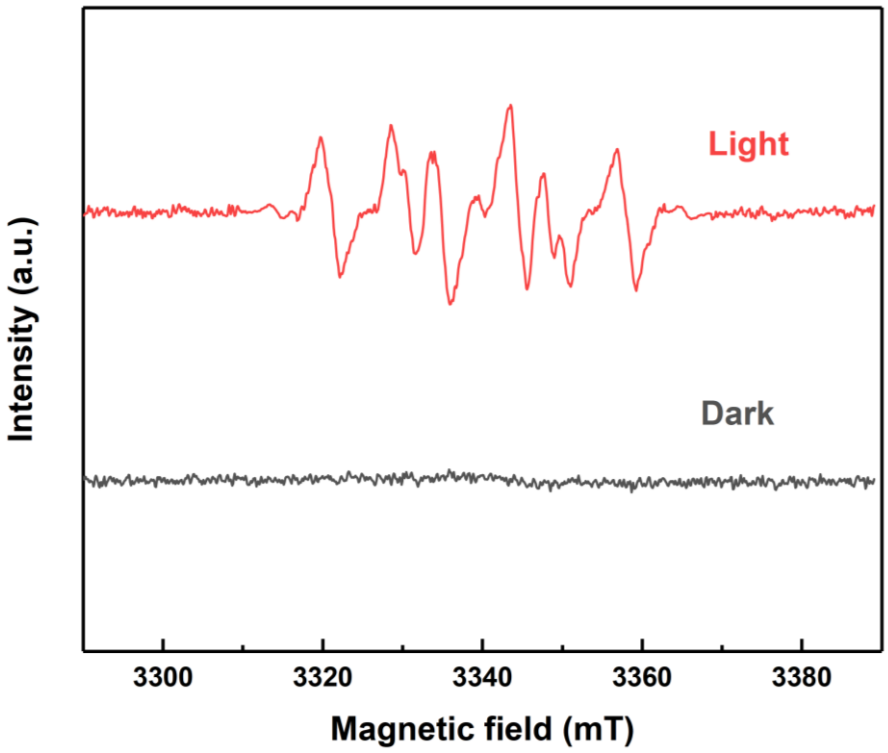


**Fig. S19** EPR spectra of HCP-DiAn in MeOH with DMPO as the trapping agent under 420 nm blue light irradiation and dark conditions.

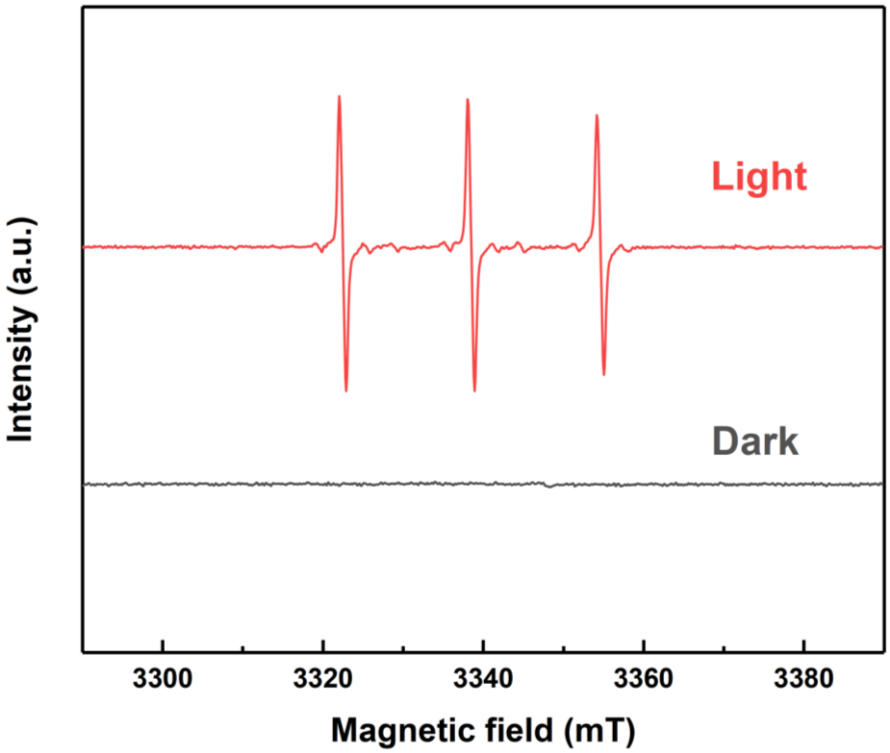


**Fig. S20** EPR spectra of HCP-DiAn in MeOH with TEMPO as the trapping agent under 420 nm blue light irradiation and dark conditions.

**Table S1**. Crystal data and structure refinement for DiBrAn.

| | |
|---|---|
| **Identification code** | 2256775 |
| **Empirical formula** | $C_{28}H_{18}Br_2$ |
| **Formula weight** | 514.24 |
| **Temperature/K** | 99.99(10) |
| **Crystal system** | monoclinic |
| **Space group** | $P2_1/n$ |
| **a/Å** | 16.0968(4) |
| **b/Å** | 8.4996(2) |
| **c/Å** | 16.1971(4) |
| **α/°** | 90 |
| **β/°** | 117.102(3) |
| **γ/°** | 90 |
| **Volume/Å$^3$** | 1972.70(10) |
| **Z** | 4 |
| **$\rho_{calc}$g/cm$^3$** | 1.731 |
| **μ/mm$^{-1}$** | 5.298 |
| **F(000)** | 1024.0 |
| **Radiation** | CuKα (λ = 1.54184) |
| **Index ranges** | $-19 \leq h \leq 14$, $-9 \leq k \leq 10$, $-18 \leq l \leq 19$ |
| **Reflections collected** | 14540 |
| **Independent reflections** | 3477 [$R_{int}$ = 0.0296, $R_{sigma}$ = 0.0250] |
| **Data/restraints/parameters** | 3477/0/271 |
| **Goodness-of-fit on F$^2$** | 1.155 |
| **Final R indexes [I>=2σ (I)]** | $R_1$ = 0.0280, $wR_2$ = 0.0713 |
| **Final R indexes [all data]** | $R_1$ = 0.0299, $wR_2$ = 0.0722 |

**Table S2**. Result of Hall measurement for HCP-DiBrAn and HCP-DiAn.

| Sample | Temp. (K) | Electrical resistance (Ω cm) | Mobility ($cm^2$ $V^{-1}$ $S^{-1}$) | Concentration of carriers ($cm^{-3}$) | Hall coefficient ($cm^3$ $C^{-1}$) | F-factor |
|---|---|---|---|---|---|---|
| HCP-DiBrAn | 300 | 0.178 | 20.9 | 1.67E+18 | -37.3 | 0.816 |
| HCP-DiAn | 300 | 0.347 | 10.7 | 1.53E+18 | -28.0 | 0.386 |

**Table S3**. Comparison of the photocatalytic performance of HCP-DiBrAn with reported materials.

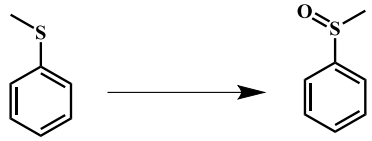

| Catalyst | Conditions | T (h) | Yield (%) | Ref. |
|---|---|---|---|---|
| $Zr_6$-Irphen | 100 W Blue LED, $O_2$ | 6 | 98 | [2] |
| $Zr_{12}$-NBC | Blue LED, Air | 10 | 100 | [3] |
| PS-HCP-4 | 210 W Xe lamp, $O_2$ | 8 | 92 | [4] |
| CF-HCP | 100 W Green LED, $O_2$ | 6 | 99 | [5] |
| P25-$TiO_2$ | TEA, 300 W Xe lamp, $O_2$ | 10 | 84 | [6] |
| In-MOF | Visible light, $H_2O_2$ | 4 | 94 | [7] |
| $TiO_2$@PDA | TEMPO, 3W blue LED, Air | 6 | 70 | [8] |
| AQ-COF | Visible light, $O_2$ | 3 | 96 | [9] |
| PPET3-$N_2$ | 3.8 mW/cm$^2$ LED, Air | 8 | 99 | [10] |
| pTCT | 26 W white CFL, Air | 12 | 95 | [11] |
| **HCP-DiBrAn** | **20 W 420 nm LED, Air** | **3** | **96** | **This work** |

## References


1. Z. Zhao, M. Liu, K. Zhou, L. Guo, Y. Shen, D. Lu, X. Hong, Z. Bao, Q. Yang, Q. Ren, P. R. Schreiner and Z. Zhang, *ACS Appl. Mater. Interfaces*, 2023, **15**, 6982-6989.
2. L.-Q. Wei and B.-H. Ye, *ACS Appl. Mater. Interfaces*, 2019, **11**, 41448-41457.
3. X.-N. Zou, D. Zhang, T.-X. Luan, Q. Li, L. Li, P.-Z. Li and Y. Zhao, *ACS Appl. Mater. Interfaces*, 2021, **13**, 20137-20144.
4. G. Ji, Z. Yang, X. Yu, Y. Zhao, F. Zhang and Z. Liu, *ACS Sustain. Chem. Eng.*, 2020, **8**, 16320-16326.
5. Y. Zhi, K. Li, H. Xia, M. Xue, Y. Mu and X. Liu, *J. Mater. Chem. A*, 2017, **5**, 8697-8704.
6. X. Lang, W. Hao, W. R. Leow, S. Li, J. Zhao and X. Chen, *Chem. Sci.*, 2015, **6**, 5000-5005.
7. H. Wei, Z. Guo, X. Liang, P. Chen, H. Liu and H. Xing, *ACS Appl. Mater. Interfaces*, 2019, **11**, 3016-3023.
8. J.-L. Shi and X. Lang, *Chem. Eng. J.*, 2020, **392**, 123632.
9. Q. Li, X. Lan, G. An, L. Ricardez-Sandoval, Z. Wang and G. Bai, *ACS Catal.*, 2020, **10**, 6664-6675.
10. J. Li, Z. An, J. Sun, C. Tan, D. Gao, Y. Tan and Y. Jiang, *ACS Appl. Mater. Interfaces*, 2020, **12**, 35475-35481.
11. J. Luo, J. Lu and J. Zhang, *J. Mater. Chem. A*, 2018, **6**, 15154-15161.